Variable-angle correlation spectroscopy in solid-state nuclear magnetic resonance

Lucio Frydman, Gerard C. Chingas, Young K. Lee,[a] Philip J. Grandinetti,
Margaret A. Eastman, Geoffrey A. Barrall, and Alexander Pines[b]
Material Sciences Division, Lawrence Berkeley Laboratory, and Department of Chemistry, University of California, Berkeley, California 94720

We describe here a new solid-state nuclear-magnetic-resonance (NMR) experiment for correlating anisotropic and isotropic chemical shifts of inequivalent nuclei in powdered samples. Spectra are obtained by processing signals arising from a spinning sample, acquired in *independent* experiments as a function of the angle between the axis of macroscopic rotation and the external magnetic field. This is in contrast to previously proposed techniques, which were based on sudden mechanical flippings or multiple-pulse sequences. We show that the time evolution of variable-angle-spinning signals is determined by a distribution relating the isotropic frequencies of the spins with their corresponding chemical shift anisotropies. Fourier transformation of these data therefore affords a two-dimensional NMR spectrum, in which line shapes of isotropic and anisotropic interactions are correlated. Theoretical and experimental considerations involved in the extraction of this spectral information are discussed, and the technique is illustrated by an analysis of ^{13}C NMR anisotropy in glycine, cysteine, and *p*-anisic acid.

I. INTRODUCTION

Cross-polarization–magic-angle-spinning (CPMAS) with high-power proton decoupling[1,2] has been widely used to obtain high-resolution NMR spectra of dilute spin-1/2 nuclei in solids.[3] Since this experiment averages anisotropies that transform as second-rank spherical harmonics, it provides spectra in which the isotropic values of chemical shifts can be measured. Valuable information, however, is also available from the principal elements of the chemical shift anisotropy (CSA) tensor, and attempts to recover these parameters from high-resolution solid-state NMR spectra appeared almost simultaneously with the first examples of the CPMAS technique.[4,5] Among the different reconstruction schemes that have been proposed to retrieve the anisotropic information, there are two approaches which involve only minor modifications of the conventional MAS experiment. In one case, CSA parameters are extracted from the spectral line shapes observed when samples are rotated slightly off the magic angle,[5-7] while in the other they are obtained from the spinning sidebands patterns observed in slow-spinning MAS spectra.[5,8,9] Despite their experimental convenience and the high-quality data that they can afford, these methods share a problem faced by one-dimensional NMR approaches in the characterization of chemical shift anisotropies: accurate values of CSA parameters can only be obtained at the expense of a partial loss in the spectral resolution.

These limitations can be avoided if two-dimensional (2D) NMR methods are used for resolving anisotropic line shapes according to the isotropic frequencies of the individual sites. The different experiments proposed for correlating these two interactions can be classified into two groups: the ones that modulate interactions by reorienting the sample, and those that manipulate the interactions using transformations in spin as well as in ordinary space. In the first group of experiments isotropic and anisotropic interactions become correlated by imposing a sudden change in the physical status of the sample, involving either a change in the axis of sample spinning,[10] in the spinning speed of the sample,[11] or in the orientation of a static sample with respect to the magnetic field.[12] In the second group of techniques, CSA interactions are reintroduced in the isotropic MAS Hamiltonian of the rotating sample by means of a multiple-pulse sequence synchronized with the spinning of the rotor.[4,13-15]

The present paper describes an alternative technique for correlating the CSA line shapes with the isotropic chemical shifts of nuclei in powdered solids. In order to obtain these 2D NMR spectra, a set of free-induction decay (FID) signals arising from a spinning sample is recorded as a function of the angle between the axis of macroscopic rotation and the external magnetic field. Since this way of acquiring data involves no sudden switching between isotropic and anisotropic interactions, the experiment is technically very simple and signal-to-noise ratios in the resulting spectra are not affected by spin-diffusion or short longitudinal relaxation times. Unlike rotor-synchronized experiments, no special sampling conditions are imposed in either of the correlated dimensions. In Sec. II we discuss the principles involved in this 2D variable-angle correlation spectroscopy (VACSY) technique. Section III describes the experimental setup that was used in order to test the predictions of the theoretical formalism, Sec. IV discusses its implementation on different samples, and Sec. V analyzes the effects of imperfections on the

[a] Graduate Group in Biophysics and the Chemical Biodynamics Laboratory, University of California, Berkeley, CA 94720.
[b] To whom correspondence should be addressed.

A

B
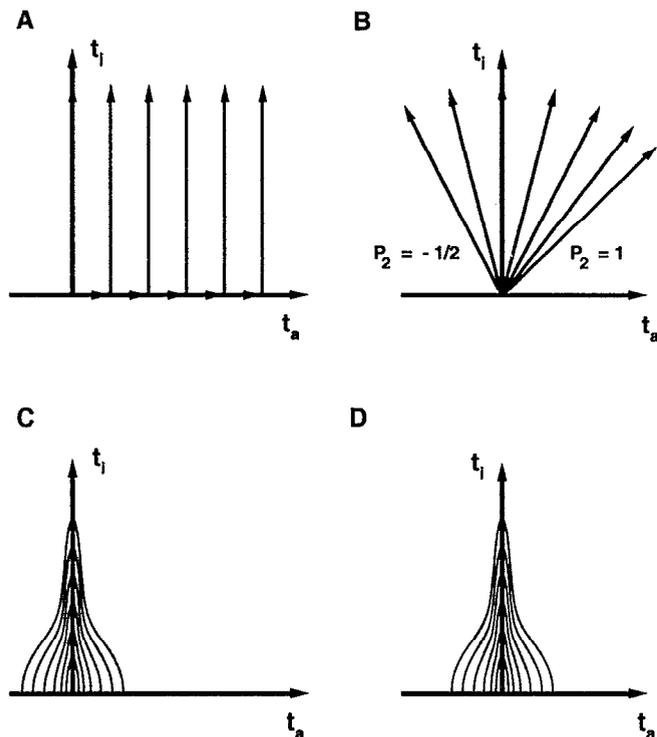
$P_2 = -1/2$ $P_2 = 1$

C

D

FIG. 1. Different approaches for correlating isotropic and anisotropic chemical shifts in solids. (A) Cartesian approach: the spin system is allowed to evolve during a time t_a under the effects of one of the interactions (in this case, the anisotropic); data are subsequently acquired as a function of an independent time parameter t_i during which the system evolves under the second interaction (the isotropic). The evolution time is incremented and the procedure repeated. (B) Mixed-dimensions approach: the direction along which the system evolves in the (t_a, t_i) plane is varied between the two indicated values $P_2(\cos \beta) = -0.5$, $P_2(\cos \beta) = 1$, by changing the spinning axis angle β. Shaded areas in (C) and (D) illustrate the portion of the signal $S(t_a, t_i)$ (shown in contours) accessible by schemes (A) and (B), respectively.

outcome of the 2D NMR correlation spectra. Finally, we briefly discuss the advantages of the present approach over previously proposed techniques.

II. THE 2D VAS NMR EXPERIMENT

Suppose that one wishes to obtain the 2D NMR spectrum of a sample in which unscaled isotropic frequencies of different sites were correlated with their corresponding full CSA powder line shapes. The usual recipes of multidimensional NMR suggest an experiment in which spins are allowed to evolve during a time t_a under the exclusive effects of the anisotropic interactions, followed (or preceded) by a time t_i in which the spins only precess at their isotropic frequencies. Regardless of the way in which these two interactions are separated, this acquisition scheme creates a time-domain space (t_a, t_i), associated with independent anisotropic and isotropic evolution frequencies. The sampling of this time domain during the course of the 2D experiment is illustrated in Fig. 1(A). From the properly digitized signal $S(t_a, t_i)$, the final correlation spectrum $I(\omega_a, \omega_i)$ can be calculated as

$$I(\omega_a, \omega_i) = \int \int S(t_a, t_i) \exp[-i(\omega_a \cdot t_a + \omega_i \cdot t_i)] dt_a dt_i .$$

(1)

This Fourier transformation provides a 2D NMR spectrum in which slices extracted parallel to the ω_a axis at the isotropic frequencies of the resolved sites show a traceless powder pattern line shape from which CSA parameters can easily be extracted.

An NMR experiment like this, involving complete separation of unscaled isotropic and anisotropic interactions, would probably be extremely impractical. However, it is possible, and even relatively simple, to measure the time-domain signals that it would generate by acquiring a set of variable-angle-spinning (VAS) NMR signals. Indeed, consider a system composed of isolated spin-1/2 nuclei spinning at an angle β with respect to the external magnetic field. In the fast-spinning regime, where the rate of sample rotation is larger than the magnitude of the CSA interaction and the effects of time-dependent terms can be disregarded, the instantaneous precession frequency of the spins ω can be approximately written as

$$\omega \approx \omega_i + P_2(\cos \beta) \cdot \omega_a(\theta, \phi).$$

(2)

In this equation, ω_i is the difference between the isotropic chemical shift of the nuclei and the transmitter offset,

$$P_2(\cos \beta) = (3 \cos^2 \beta - 1)/2$$

(3)

is the second-order Legendre polynomial of $\cos \beta$, and

$$\omega_a(\theta, \phi) = (\Delta \omega/2)(3 \cos^2 \theta - 1 + \eta \sin^2 \theta \cos 2\phi)$$

(4)

denotes the anisotropic frequency of the spins, depending on the CSA parameters $\Delta \omega$ and η and on two Euler angles (θ, ϕ) relating the principal axis system of each crystallite with a reference frame fixed on the rotor. Although the transformations represented by their angles are different, the powder pattern distribution of ω_a in Eq. (4) is identical to the one arising from the ω_a appearing in Eq. (1). For any particular value of $P_2(\cos \beta)$ scaling the anisotropic interactions in Eq. (2), the signal observed at a time t after exciting the spins in the rotating sample can therefore be written as

$$S(\beta, t) = \int \int I(\omega_a, \omega_i) \exp\{i[\omega_a \cdot P_2(\cos \beta) t + \omega_i \cdot t]\}$$

$$\times d\omega_a d\omega_i .$$

(5)

By replacing in this expression

$$t_a = P_2(\cos \beta) t$$

(6)

and

$$t_i = t,$$

(7)

it is possible to rewrite the signal arising from the system as

$$S(t_a, t_i) = \int \int I(\omega_a, \omega_i) \exp[i(\omega_a \cdot t_a + \omega_i \cdot t_i)] d\omega_a d\omega_i .$$

(8)

According to Eqs. (6)–(8), the spectrum $I(\omega_a, \omega_i)$ correlating the isotropic chemical shifts with CSA line

shapes forms a 2D Fourier pair with a set of signals acquired as a function of β and t. Although these two experimental variables are not capable of explicitly separating isotropic and anisotropic interactions, they do provide a way of sampling the (t_a, t_i) space associated with them. Figure 1(B) illustrates the roles played by β and t in the acquisition of the $S(t_a, t_i)$ signals, as well as the region of the (t_a, t_i) space that can be sampled by changing the orientation of the sample spinning axis with respect to the magnetic field. This figure reveals the underlying similarity between the way in which spinning angles β sweep the (t_a, t_i) space, and the way in which gradients sample the (k_x, k_y) domain in 2D projection-reconstruction experiments.[16] Since arbitrary changes in the values of the (G_x, G_y) imaging gradients allow one to acquire data over the complete (k_x, k_y) space, the time-domain signal can be related to the spin density in the (x, y) space by back-projection methods.[17] Here, however, the $-0.5 \leqslant P_2(\cos \beta)$ $\leqslant 1$ constraint restricts VAS measurements to the region indicated in Fig. 1(B), and therefore the 2D spectrum that can be obtained by inversion of Eq. (8),

$$I(\omega_a, \omega_i) = \int_0^\infty \int_{-t_i/2}^{t_i} S(t_a, t_i) \exp[-i(\omega_a \cdot t_a + \omega_i \cdot t_i)]$$

$$\times dt_a dt_i, \tag{9}$$

is only an approximation to the ideal correlation spectrum introduced in Eq. (1). Similar approximations, however, are involved in several conventional 2D NMR schemes, which also restrict measurement of the signal to a limited region of the time domain. Figures 1(C) and 1(D) compare regions of (t_a, t_i) space that are sampled in conventional (nonecho) 2D and in VACSY NMR experiments, illustrating the data truncation occurring for a system evolving under the effects of combined anisotropic-isotropic interactions. In both cases regions of maximum signal intensity neighboring the t_i axis are sampled, and Fourier analysis of either set of data will afford a very good approximation to the actual $I(\omega_a, \omega_i)$ distributions. In the case shown in Fig. 1(C), truncation of the $S(t_a, t_i)$ signal results in the sinc wiggles and phase-twisted peaks familiar in 2D NMR spectroscopy. Similarly, time-domain truncation in the present case [Fig. 1(D)] produces its own distinctive artifacts, which appear as small diagonal ridges running off each $I(\omega_a, \omega_i)$ peak. As shown below, however, the magnitude of this effect is rather small, so use of Eq. (9) is satisfactory.

III. EXPERIMENT

A. Data acquisition and processing

A straightforward way of evaluating Eq. (9) is the fast-Fourier-transform algorithm, which requires an equally spaced grid of data points for relating the time-domain data with the frequency spectra. An obvious way of generating this array is by adjusting the values of β and dwell times used in the acquisitions, to sample all points on a regular grid in (t_a, t_i) space. This procedure, however, is highly inefficient, as it requires an excessively large number
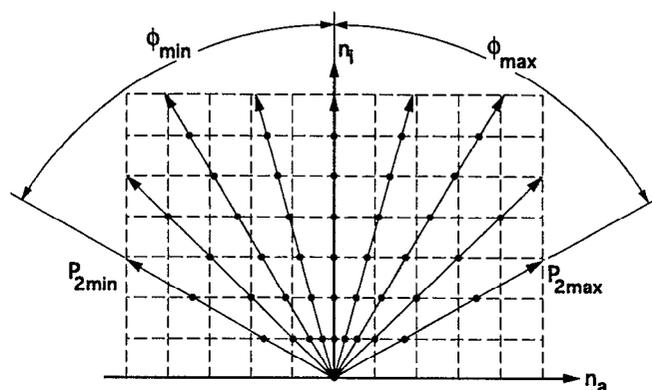

FIG. 2. Strategy employed for obtaining isotropic–anisotropic correlation spectra from 2D VAS NMR data. The arrows represent individual FID's involved in the 2D acquisition; the dashed grid represents the desired regular array to be Fourier transformed. Sampling of the signal in the different VAS experiments, represented by the dots, takes place at integer multiples of the physical dwell time, which determines the grid spacing along the n_i axis (DW$_i$). $P_{2\text{max}}$ and $P_{2\text{min}}$, the two extrema of $P_2(\cos \beta)$ used in the acquisition, determine a wedge in (n_a, n_i) space bound by angles ϕ_{max} and ϕ_{min}. Spinning angles $\{\beta_i\}$ are then selected so that the acquisition rays are evenly distributed between ϕ_{max} and ϕ_{min}. Interpolation of data values is carried out for all the grid points falling inside the wedge.

of β values even for sampling relatively small data grids. A more efficient approach consists of selecting a region in the (t_a, t_i) space capable of supporting the desired spectral resolution, and sampling it using only as many different angles β as are necessary to ensure accurate interpolation of the time-domain grid. This procedure, illustrated in Fig. 2, was the one that we adopted to retrieve $I(\omega_a, \omega_i)$ spectra.

As in conventional 2D NMR, range and resolution in the final 2D VACSY spectra are determined by the spacing and the total number of points in the time-domain grid. We specify the density of the grid in terms of "dwell times" DW$_a$ and DW$_i$, denoting the time increments between adjacent points along the t_a and t_i directions. According to Eq. (7), sufficient resolution along the ω_i direction can be ensured by setting the actual dwell times equal to DW$_i$ for all VAS acquisitions. The spinning angle β provides the additional degree of freedom, by mapping each acquired signal on a ray in (t_a, t_i) space. To sample these rays uniformly, we determine the acquisition geometry not directly in the (t_a, t_i) space but rather on the "grid space" (n_a, n_i) where the final time-domain data are located, and in which distances are scaled by units of DW$_a$ along the t_a axis and DW$_i$ along the t_i axis. Coverage limitations arise at this point, as $P_2(\cos \beta)$ cannot extend beyond $-1/2$ and $+1$ regardless of the spinning angle. Data are therefore restricted to a wedge in (n_a, n_i) space limited on the sides by the two experiments performed with the highest and lowest values of $P_2(\cos \beta)$, $P_{2\text{max}}$, and $P_{2\text{min}}$ (Fig. 2). The angles ϕ_{max} and ϕ_{min} that in the final data matrix these experiments subtend with the isotropic axis are given by

$$\tan(\phi_{\text{max}}) = \text{DW}_i / (\text{DW}_a \cdot P_{2\text{max}}), \tag{10a}$$

$$\tan(\phi_{\text{min}}) = \text{DW}_i / (\text{DW}_a \cdot P_{2\text{min}}). \tag{10b}$$

Given N independent VAS experiments, the angles ϕ_i involved in a uniform sampling of the (t_a, t_i) space can be obtained from Eqs. (10) as

$$\phi_i = \phi_{\min} + (\phi_{\max} - \phi_{\min}) \frac{i-1}{N-1}, \quad i = 1,2,...,N. \quad (11)$$

This set $\{\phi_i\}$ determines the actual value of the angles $\{\beta_i\}$ used in the 2D VAS experiment according to

$$\beta_i = \cos^{-1} \left[\frac{2 \cdot DW_a \cdot \tan(\phi_i)/DW_i + 1}{3} \right]^{1/2},$$

$$i = 1,2,...,N. \quad (12)$$

We have found empirically that for $-0.5 \leqslant P_2(\cos \beta_i) \leqslant 0.5$, satisfactory spectra can be obtained with N as low as 30. It is likely that sampling considerations applied to back-projection schemes are also applicable to VACSY experiments, but a rigorous analysis of this point is beyond the scope of the present work.

Once the 2D experiment is completed, the acquired data are used to interpolate a regular array in the region between $\phi_{\min}$ and $\phi_{\max}$. Since signals corresponding to different spinning angles are digitized using equal dwell times DW_i, the positions on the grid to be interpolated are flanked along their t_a coordinates by two data points (see Fig. 2). These points were used to linearly interpolate the signal for intermediate positions on the regular array, until a dense grid of data was generated. The total number of points interpolated along the two dimensions of the grid that is Fourier transformed is somewhat arbitrary; the main requirement being that it should be large enough to allow the signal to decay completely in order to support maximum resolution. In the present studies the interpolated matrix was truncated to a rectangular shape similar to the one formed by the heads of the arrows shown in Fig. 2.

B. NMR measurements

The predictions of the preceding paragraphs were tested by recording the ^{13}C CP NMR spectra of a series of compounds in a 4.2 T superconducting magnet at a resonance frequency of 45.2 MHz. The NMR spectrometer that was used is based on a Tecmag pulse-programmer and data-acquisition systems, and on home-built rf accessories. The probehead employed for carrying out the measurements is a single-coil double-tuned system, described elsewhere in detail.[18] A conventional CP sequence with phase inversion of the initial decoupler 90° pulse and flip-back pulse was used to acquire the signals. Hartmann–Hahn matching was achieved at ca. 80 kHz using 200 W in the transmitter channel and 100 W in the decoupler channel.

The stator of the probe is coupled to a stepping motor located at the base of the magnet, which allowed us to set the angle between the spinning axis of the rotor and the external magnetic field to within 0.088° resolution (1 part in 4096). The motor controller was carefully referenced to the magic angle prior to each 2D acquisition by maximizing rotational echoes in a ^{81}Br FID of solid KBr. The angles required for acquiring the complete 2D set were
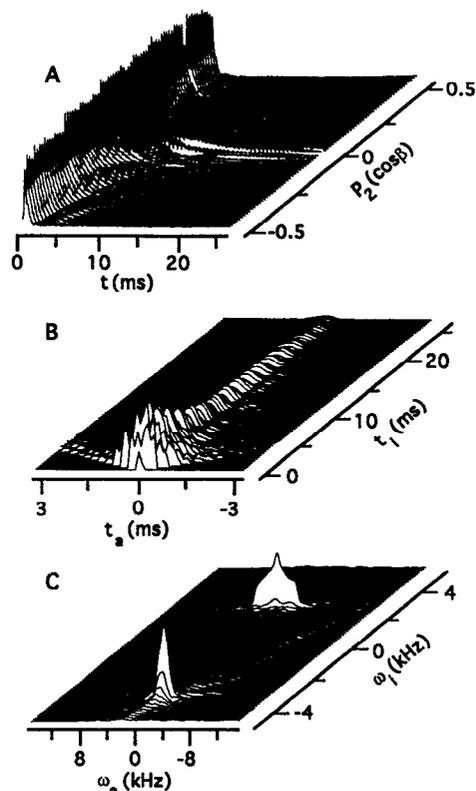

FIG. 3. Stack plots of the different data processing stages involved in a 2D VAS correlation experiment performed on a glycine sample. (A) Set of 75 FID's recorded as a function of a set of Legendre polynomials $\{P_2(\cos \beta_i)\}$ given by Eq. (12) for $DW_i/DW_a = 4$, sampled using 256 points and a 10^{-4} s physical dwell time. (B) 2D set obtained after interpolating the experimental data on a regular grid composed by 128×256 points. (C) Isotropic–anisotropic correlation spectrum obtained by 2D Fourier transformation of the set shown in (B), after zero filling to 256×512 points.

calculated before the beginning of each experiment, and automatically updated by the acquisition program. Since the rf coil of the probe is fixed around the stator the signal-to-noise ratio of the acquired signal deteriorates as β approaches 0. Therefore we restricted the orientation of the spinning axis to the range $-0.5 \leqslant P_2(\cos \beta) \leqslant 0.5$, so that in all the experiments described below $\phi_{\max} = -\phi_{\min} = \tan^{-1}(2DW_i/DW_a)$. After completing the acquisition, the full 2D set was transferred to a μVAX2 workstation and processed as described above.

IV. RESULTS

Figure 3 illustrates the different stages taking place as 2D VACSY NMR data are processed to yield an isotropic–anisotropic correlation spectrum for the case of glycine. The plot in Fig. 3(A) shows the 2D set of FID's acquired for this sample as a function of the spinning angle over the range $-0.5 \leqslant P_2(\cos \beta) \leqslant 0.5$. These signals were used to estimate the values of $S(t_a, t_i)$ over a grid of regularly distributed points; the results of this interpolation are shown in Fig. 3(B). Since the (t_a, t_i) plane was covered using both positive and negative values of $P_2(\cos \beta)$, the data appear
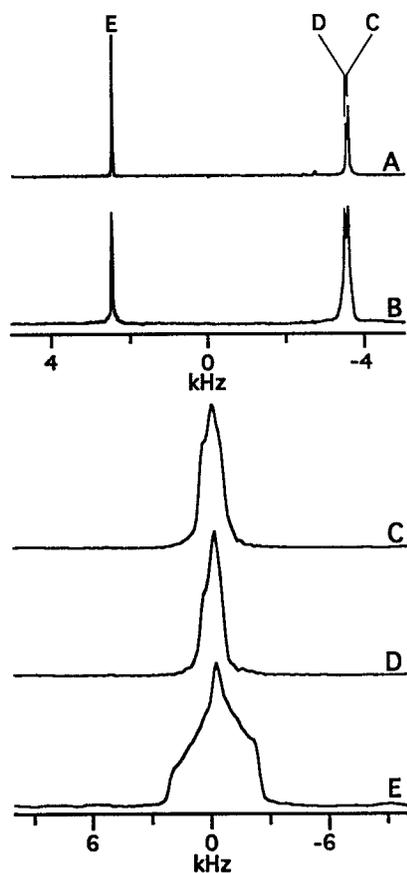
FIG. 4. (A) Normal ^{13}C CPMAS NMR spectrum of glycine. (B) Isotropic slice extracted at $\omega_a=0$ from the 2D spectrum shown in Fig. 3(C). Both (A) and (B) spectra originate from 256-point signals that were zero filled to 512 points before transformation. Their origin of frequencies is placed at the carrier offset of the transmitter. (C)–(E) Powder line shapes afforded by slices of the 2D glycine spectrum shown in Fig. 3(C), extracted parallel to the ω_a axis at the isotropic frequencies labeled in the MAS spectrum. Note that peaks C and D arising from the carbon bonded to the nitrogen have different linewidths, probably due to the different dipolar broadenings introduced by the ^{14}N state associated with each.

as a series of t_a echoes obtained for positive values of t_i. As in conventional 2D NMR this echo will cancel the dispersive components appearing along the ω_a axis in the frequency domain, simplifying the calculation of pure-phase $I(\omega_a,\omega_i)$ spectra. The ratio between isotropic and anisotropic dwell times chosen in Eqs. (10) for acquiring the data is also reflected in the interpolated set, as it gives rise to ridges of truncated data departing from the time origin at angles $\phi_{max}=-\phi_{min}=63.4$ with respect to the t_i axis. At this stage conventional apodization and zero filling along both domains can be applied to the signal; 2D Fourier transformation and phasing affords the final correlation spectrum $I(\omega_a,\omega_i)$ of glycine [Fig. 3(C)]. This spectrum presents all the features that could have been expected from the discussion in Sec. II, apart from the minor artifacts appearing in the form of small diagonal ridges emerging from the peaks. The resolution observed along the isotropic axis is similar to the one displayed by the normal absorption MAS spectrum of glycine [Figs. 4(A) and
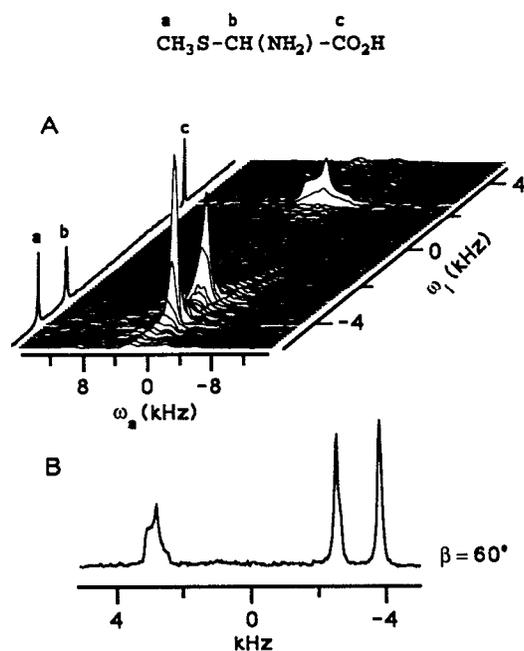

$$CH_3S-CH(NH_2)-CO_2H$$

FIG. 5. (A) 2D VAS isotropic–anisotropic correlation spectrum of cysteine, showing the projection along the isotropic axis and the assignment of the peaks to the different sites in the molecule. 97 FID's were acquired as a function of the spinning angle β, and were interpolated to a 128×256 time-domain data set, which was Fourier transformed to give the final spectrum. Other acquisition parameters are as in Fig. 3. (B) ^{13}C CP NMR spectrum of cysteine recorded on a sample spinning at an angle of 60° with respect to the magnetic field. Note the similarity between the line shape of the carbonyl peak in this spectrum and the one afforded by the 2D VAS correlation experiment.

4(B)]. Slices of the 2D spectrum extracted parallel to the ω_a axis provide the resolved CSA powder patterns for each of the peaks, from which the principal values of the now traceless interaction can be obtained [Figs. 4(C)–4(E)].

Slightly different results were observed when the 2D VACSY spectrum of cysteine was recorded [Fig. 5(A)]. In this spectrum, the anisotropic line shape arising from the carbons of the carboxylic group is different from an ideal powder pattern, although its singularities appear at values similar to the ones observed for the same group in glycine. When the individual VAS spectra of cysteine acquired during the course of the 2D experiments were investigated, it was found that in all cases where peaks could be resolved the scaled powder patterns of the carboxylic group also showed this deformation [Fig. 5(B)]. This indicates that the features observed in the $I(\omega_a,\omega_i)$ spectrum are not a consequence of the particular way in which data were acquired or processed, but reflect instead an intrinsic property of the sample. Similar deviations from the expected line shapes were observed for nonprotonated carbon peaks in other compounds. This indicates that, as is probably the case in all types of isotropic–anisotropic correlation experiments, one of the main factors distorting anisotropic line shapes will be related with the efficiency of the cross-polarization process.[1,19]

Figure 6 shows a correlation spectrum between isotropic and anisotropic chemical shifts obtained on a sample of
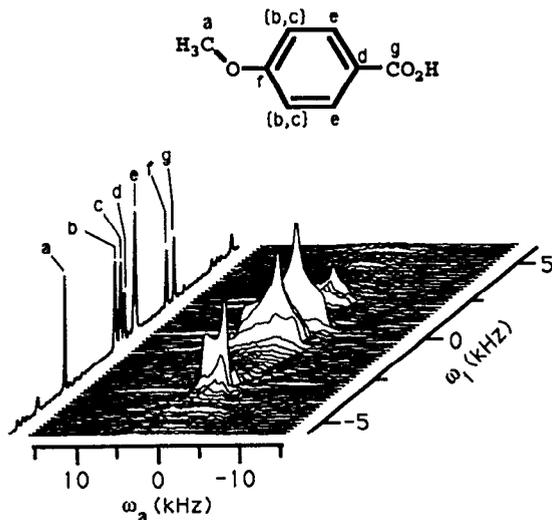
FIG. 6. 2D isotropic–anisotropic NMR correlation spectrum of *p*-anisic acid, showing the isotropic projection and the assignment of the peaks to each of the sites in the molecule. An ambiguity remains concerning peaks b and c, the signals arising from the carbons *ortho* to the OCH$_3$ group. Sampling of the data afforded a spectral window of 12 kHz along the isotropic axis; other experimental parameters are as in Fig. 3. The small peaks appearing without label at high and low frequencies of the main resonances are spinning sidebands.

p-anisic acid. Although in solution the ^{13}C NMR spectrum of this compound displays six inequivalent carbon peaks, solid-state effects introduce an additional splitting in the signal arising from the aromatic carbons *ortho* to the –OCH$_3$ group. The resulting seven resonances are clearly resolved. An analysis of the slices that can be extracted parallel to the ω_a axis at the isotropic frequencies of the different peaks is presented in Fig. 7. Each resolved site provides the singularities of the CSA patterns, which were used to simulate the expected powder distributions. As happened to be the case with cysteine the main deviations between theoretical and experimental line shapes occur for the nonprotonated carbon resonances but, even for these sites, measurement of the principal values of the CSA tensors is straightforward. A complete list of these values is summarized in Table I.

V. DISCUSSION

A. Slow-spinning effects

Throughout the present study, we assumed the sample to be spinning fast enough to allow us to disregard the effects of time-dependent terms modulating the precession frequencies of the spins. Nevertheless, the presence of spinning sidebands in Fig. 6 show that this fast-spinning assumption was not strictly fulfilled, so an analysis of the effects of slow spinning on the outcome of the experiment was carried out. Powder signals for individual spinning sites were calculated for a set of angles $\{\beta_i\}$, and processed as above to yield isotropic–anisotropic correlation NMR spectra. Results of these calculations are presented in Fig. 8, as a function of the spinning speed of the sample. As can
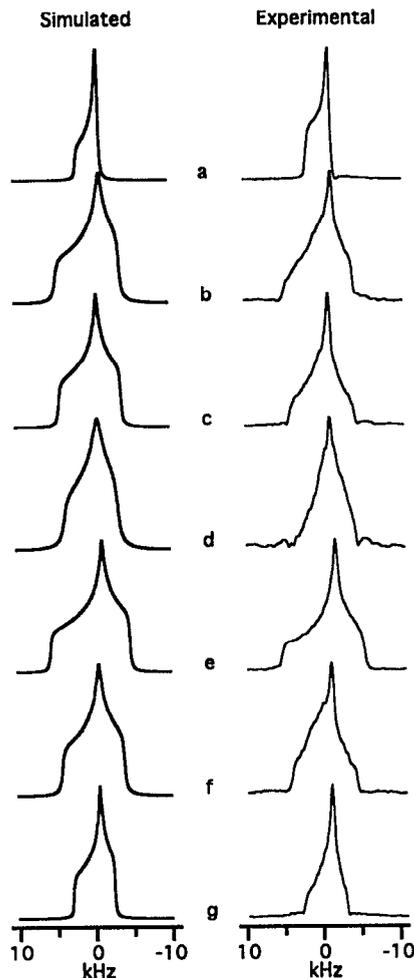

FIG. 7. Experimental and simulated line shapes obtained from slices extracted at the isotropic frequencies of the peaks of *p*-anisic acid. Each pair of spectra corresponds to the carbon labeled with the same letter in Fig. 6. Simulations were obtained using the three singularities that can be read from the experimental line shapes.

be seen the spinning sidebands appear as sharp peaks along the isotropic dimension, but show broad powder line shapes along the anisotropic axis. Figure 9 shows the changes in the anisotropic patterns of the center-band peaks as a function of the spinning speed. Deviations from the static line shape appear as the spinning rate is reduced, with a behavior reminiscent of that observed when off-

TABLE I. ^{13}C NMR shielding parameters in *p*-anisic acid.[a]

Carbon atom	$\Delta\omega$ (ppm)	η
a	−42.0	0.16
b	−104.0	0.55
c	−96.2	0.72
d	−83.0	0.71
e	−126.1	0.63
f	−95.1	0.77
g	−65.3	0.63

[a]Assuming $\omega_{11} > \omega_{22} > \omega_{33}$; $\omega_{11} + \omega_{22} + \omega_{33} = 0$. Principal values are considered accurate within ±1 ppm.

ν_r (Hz)

417
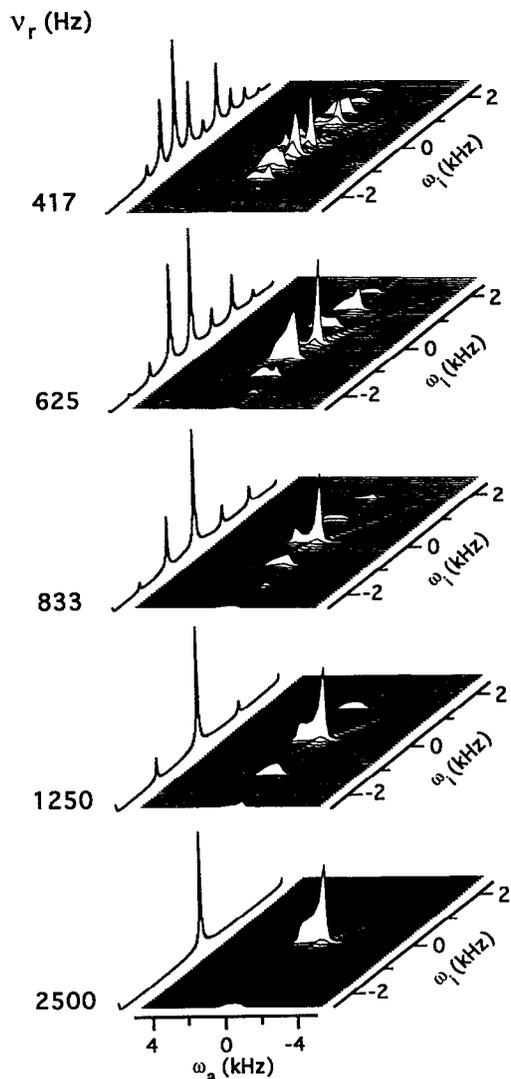
625

833

1250

2500

ω_a (kHz)

4   0   -4

FIG. 8. Simulation of the results afforded by the 2D VAS correlation experiment on a single-site sample rotating at different spinning speeds. The numbers to the left of each spectrum indicate the spinning speed used in the calculations. CSA parameters used to simulate the spectra are $\omega_i=0$ Hz, $\Delta\omega=1.4$ kHz, $\eta=0$. The 1D plots shown on the left of each simulation are the projections of the 2D sets along their isotropic axes.

ν_r (Hz)
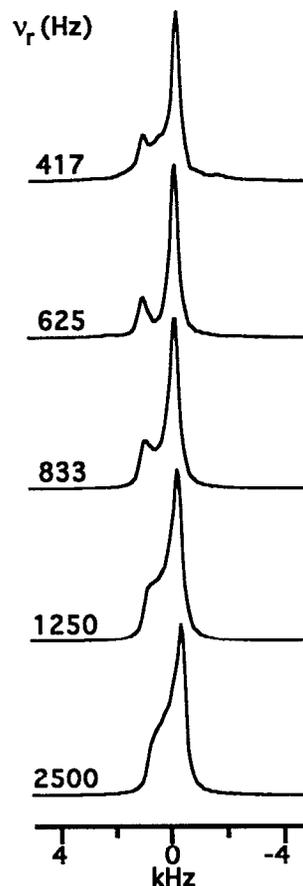
417

625

833

1250

2500

4   0   -4
kHz

FIG. 9. Slices extracted at the isotropic frequencies of the simulations shown in Fig. 8, showing the effects that changing the spinning speed can be expected to introduce in the line shapes obtained in a 2D VAS correlation experiment.

magic-angle spectra are recorded at slow spinning speeds.[20,21] Singularities corresponding to the principal values of the CSA tensor can, however, be resolved regardless of the spinning rate, rendering the 2D VACSY experiment useful even in the slow-spinning regime. The distinctive powder structures observed for the sidebands at slow spinning speeds are particularly interesting: these anisotropic patterns can be expanded in terms of orientational distributions[22] to provide insight into the molecular alignments in the sample under analysis.

B. Effects of angle missetting

The most critical instrumental error in the VACSY experiment is improper setting of the sample spinning axes. Deviations from the ideal set of $\{\beta_i\}$ angles may be either

systematic or random. Errors of the first type will appear if the initial angle, to which all other orientations in the 2D experiment are referenced, is set incorrectly. These errors can be minimized by setting the reference spinning axis spectroscopically at the magic angle as described above. This is an extremely accurate procedure whose error is usually smaller than 0.1°. Random errors, however, will always be present upon changing the orientation of the sample spinning axes during the 2D VAS experiment, due to the finite accuracy of the mechanism employed for stepping through the angles. Effects introduced by these errors on the anisotropic line shapes were computer simulated, and are presented in Fig. 10. As can be seen, neither the signal-to-noise ratio nor the position of the singularities along the anisotropic axis are significantly affected by small deviations from the ideal angles. The main effect that can be observed is a deformation in the shape of the powder patterns, which becomes severe only when the angles of sample spinning differ from their ideal values by several degrees.

VI. CONCLUSIONS

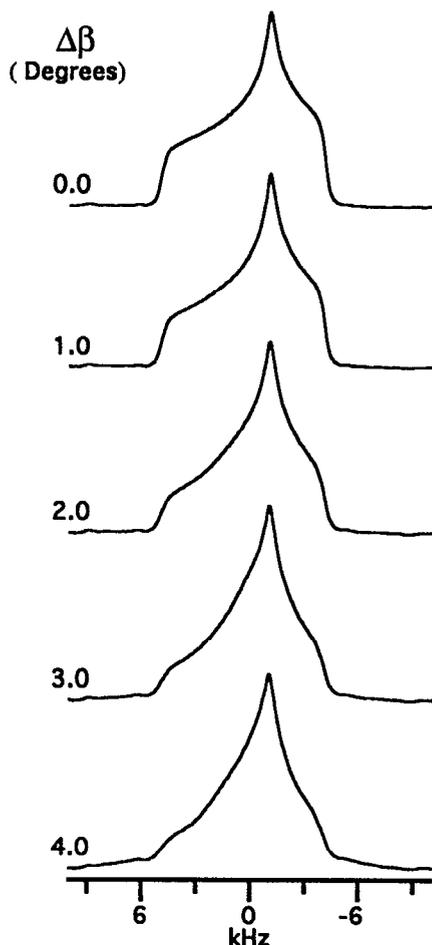In the preceding sections we have introduced a new technique for correlating isotropic chemical shifts with

FIG. 10. Effects introduced by an angle misseting $\Delta\beta$ on the anisotropic line shapes observed in a 2D VAS correlation experiment. Simulations were done for a CSA tensor characterized by $\omega_{11} = 5$ kHz, $\omega_{22} = -1$ kHz, $\omega_{33} = -4$ kHz. Errors in the spinning angles for each of the 64 acquisitions used in each simulation were introduced using a random-number generator. The range of angular errors is indicated at the left of each spectrum. Although line shapes change when errors exceed 2°, the position of the powder singularities remains constant.

chemical shift anisotropies, and demonstrated its feasibility with several examples. The implementation of the experiment is relatively simple; spectra are obtained with good signal-to-noise ratios and in a format that affords the complete chemical shift information in a straightforward way. Compared with previous methods proposed to obtain similar 2D information,[4,10-15,23] the present approach exhibits a number of advantages. In contrast to techniques that involve sudden spatial changes in the sample orientation, the present 2D VAS experiment does not require storage of evolving magnetizations. Therefore, it should afford spectra characterized by higher signal-to-noise ratios and independent of the relaxation properties of the sample. The mechanical simplicity of the VACSY experiment is compatible with very high spinning speeds, and can be easily coupled to variable-temperature operation. Furthermore, since the present approach requires neither sampling nor irradiation to be stroboscopic with the spinning speed of the rotor, it is well suited for recording spectra on samples

that require a large number of signal-averaging scans. The only drawback of the present approach is computational, as it requires an additional manipulation of the data (the interpolation) prior to obtaining the spectrum. Nevertheless, this procedure is relatively simple, and requires only a small fraction of the time involved in, for instance, the 2D Fourier transformation itself.

The most significant spectroscopic aspect of the VACSY experiment is that data are extracted by scaling rather than by switching 2D NMR interactions. By varying the spinning axis the relative magnitudes of isotropic and anisotropic evolutions are changed, thus replacing the switched-Hamiltonian approach which requires both rapid mechanical motion and magnetization storage. We are currently exploring the applications of this non-Cartesian approach for sampling multidimensional domains to additional NMR experiments, such as the extraction of CSA parameters from single crystals, correlation of anisotropic chemical shift and dipole interactions, characterization of dynamic processes, and solution experiments involving scaling or modulation of chemical shifts or J couplings.[24]

Although the techniques used in the present study are related to approaches of widespread application in NMR imaging,[25,26] their application in a purely spectroscopic context is novel. The underlying commonality between the imaging and the spectroscopic applications is a consequence of the inherently statistical aspect of NMR data. The development of well-defined phase in NMR signals generally implies that the acquired data sample a characteristic function of one or more random variables,[27] whose identity is determined by the functional form of the phase.[28] In the present case, the phase appearing in the exponent of Eq. (5) indicates that the "probability distribution" of (ω_a, ω_i)—the spectrum—will become available by Fourier analysis of the signal. Artifacts due to incompletely sampled data can then be treated as simple products of point spread functions of data "apertures," as illustrated in Figs. 1(C) and 1(D). It seems likely that these concepts, which have had such a great theoretical and practical impact on the field of NMR imaging, will also become applicable to other branches of spectroscopy as well.

ACKNOWLEDGMENTS

[1] A. Pines, M. G. Gibby, and J. S. Waugh, J. Chem. Phys. **59**, 569 (1973).
[2] J. Schaefer and E. O. Stejskal, J. Am. Chem. Soc. **98**, 1031 (1976).
[3] C. A. Fyfe, *Solid State NMR for Chemists* (CFC, Guelph, 1983).
[4] E. Lipmaa, M. Alla, and T. Turherm, Proceedings of the 19th Congress Ampere, Heidelberg, 1976 (unpublished), p. 241.

[5] E. O. Stejskal, J. Schaefer, and R. A. McKay, J. Magn. Reson. **25**, 569 (1977).

[6] A. Pines, personal communication in reference 5, 1976.

[7] N. K. Sethi, D. M. Grant, and R. J. Pugmire, J. Magn. Reson. **71**, 476 (1987).

[8] M. M. Maricq and J. S. Waugh, J. Chem. Phys. **70**, 3300 (1979).

[9] J. Herzfeld and A. E. Berger, J. Chem. Phys. **73**, 6021 (1980).

[10] A. Bax, N. M. Szeverenyi, and G. E. Maciel, J. Magn. Reson. **55**, 494 (1983).

[11] R. C. Zeigler, R. A. Wind, and G. E. Maciel, J. Magn. Reson. **79**, 299 (1988).

[12] A. Bax, N. M. Szeverenyi, and G. E. Maciel, J. Magn. Reson. **52**, 147 (1983).

[13] Y. Yarim-Agaev, P. N. Tutujian, and J. S. Waugh, J. Magn. Reson. **47**, 51 (1982).

[14] A. Bax, N. M. Szeverenyi, and G. E. Maciel, J. Magn. Reson. **51**, 400 (1983).

[15] R. Tycko, G. Dabbagh, and P. A. Mirau, J. Magn. Reson. **85**, 265 (1989).

[16] P. Mansfield and P. G. Morris, *NMR Imaging in Biomedicine*, edited by J. S. Waugh, Advances in Magnetic Resonance (Academic, New York, 1982), Suppl. 2.

[17] R. A. Brooks and G. DiChiro, Radiology **117**, 561 (1975).

[18] M. A. Eastman, P. J. Grandinetti, Y. K. Lee, and A. Pines, J. Magn. Reson. **98**, 333 (1992).

[19] C. S. Yannoni and H. E. Bleich, J. Chem. Phys. **55**, 5406 (1971).

[20] N. K. Sethi, D. W. Alderman, and D. M. Grant, Mol. Phys. **71**, 217 (1990).

[21] E. M. Menger, D. P. Raleigh, and R. G. Griffin, J. Magn. Reson. **63**, 579 (1985).

[22] G. S. Harbison, V.-D. Vogt, and H. W. Spiess, J. Chem. Phys. **86**, 1206 (1987).

[23] G. E. Maciel, N. M. Szeverenyi, and M. Sardashti, J. Magn. Reson. **64**, 365 (1985).

[24] R. V. Hosur, Prog. Nucl. Magn. Spectrosc. **22**, 1 (1990).

[25] D. B. Tweig, J. Katz, and R. M. Peshock, Magn. Reson. Med. **5**, 32 (1987).

[26] D. G. Cory, J. B. Miller, A. N. Garroway, and W. S. Veeman, J. Magn. Reson. **85**, 219 (1989).

[27] E. Parzen, *Modern Probability Theory and Its Applications* (Wiley, New York, 1960).

[28] L. Frydman, G. A. Barral, J. S. Harwood, and G. C. Chingas, Proceedings of the 1st Congress on NMR Microscopy, Heidelberg, 1992 (in press).